Imaging and Manipulation of High-Density Lipoproteins

Joseph W. Carlson,*# Ana Jonas,§ and Stephen G. Sligar*#§
*Center for Biophysics, #Beckman Institute for Advanced Science and Technology, and §Department of Biochemistry, the University of Illinois, Urbana, Illinois 61801 USA

ABSTRACT The atomic force microscope (AFM) has been used to image a variety of biological systems, but has rarely been applied to soluble protein-lipid complexes. One of the primary physiological protein-lipid complexes is the high-density lipoproteins (HDL), responsible for the transport of cholesterol from the peripheral tissues and other lipoproteins to the liver. We have used the AFM to directly image discoidal reconstituted HDL (rHDL) particles for the first time. The height of these particles is consistent with a phospholipid bilayer structure, but careful high resolution measurements of particle diameters has indicated that they fuse when adsorbed to mica. Furthermore, it has been demonstrated that the AFM can be used to initiate this bilayer fusion in a controlled manner, allowing the fabrication of stabilized, nanometer scale, phospholipid bilayer "domains."

INTRODUCTION

The role of HDL is that of a reverse cholesterol transporter, whereby excess cholesterol is removed from peripheral tissues and other lipoproteins and delivered to the liver for disposal. High-density lipoproteins are believed to exist in two forms in the circulation; a nascent discoidal form, abundant in the plasma of lecithin cholesterol acyltransferase (LCAT) deficient patients, and a mature spherical form, the predominant form in normal individuals. The spherical form is the result of transformation of discoidal HDL through the action of LCAT and plasma lipid transfer proteins. The main difficulties associated with studying the function of HDL have been related to the inability to obtain precise structural information. Difficulties in obtaining crystals of most lipoproteins and apolipoproteins have prevented the use of high-resolution x-ray crystallography. Transmission electron microscopy (TEM) of negatively stained samples (Forte et al., 1971a, b; Tall et al., 1977; Wlodawer et al., 1979; Brouillette et al., 1984) revealed both cylindrical stacks of discoidally shaped objects, called rouleaux, and circular objects, believed to be unstacked disks lying flat on the TEM grid. The rouleaux aggregates are believed to be an artifact resulting from the negative stain process, and do not reflect the solution structure of discoidal HDL (Forte et al., 1971b; Morrissett et al., 1974). The currently accepted model of nascent HDL structure is that of a phospholipid bilayer that is stabilized at its edges by amphipathic apolipoprotein helices (Segrest, 1977; Jonas, 1992). This model is further supported by neutron scattering, small angle x-ray scattering, and freeze fracture TEM data (Atkinson et al., 1976, 1980; Hamilton et al., 1976; Wlodawer et al., 1979).

The primary protein component of HDL is apolipoprotein A-I (apoA-I), which is the most potent activator of lecithin cholesterol acyltransferase (LCAT) (Fielding et al., 1972; Jonas, 1991). ApoA-I is thought to fold into a number of amphipathic helices that bind to the HDL surfaces and stabilize the lipid particles (Boguski et al., 1986; Segrest et al., 1992). The structure of the discoidal form of HDL is closely related to the structure of the protein, which, through the binding of its amphipathic helices to the acyl chains of the phospholipid, stabilizes discrete sizes of phospholipid disks (Jonas, 1992). Native high-density lipoproteins are very heterogeneous, being composed of many apolipoproteins, including apoA-I, as well as phospholipids, cholesterol esters, free cholesterol, triglycerides, and lysolecithins (Assman et al., 1992). Because of this compositional heterogeneity, the study of HDL has greatly benefited from the ability to reconstitute HDL in vitro (Matz and Jonas, 1982; Jonas, 1986). Reconstituted HDL (rHDL), while retaining many of the characteristics of native HDL, can be made with specific constituents, so that their size, phospholipid and protein composition can be controlled (Jonas et al., 1989, 1990; Wald et al., 1990).

The present investigation addresses the structure of rHDL under physiological conditions by providing the first visualization of rHDL by AFM. The structure of rHDL has been demonstrated to be a bilayer, consistent with previous investigations. The size of rHDL on the surface has been examined, and evidence presented that rHDL undergo a specific fusion and division process on the surface, where apoA-I continues to stabilize certain disk sizes over others. This fusion process occurs spontaneously and is believed to be a result of orienting the rHDL with their edges in proximity. The present investigation further demonstrates the ability of AFM to, under the appropriate conditions, induce this fusion process, allowing the fabrication of nanometer scale phospholipid bilayer domains.

Received for publication 10 March 1997 in final form 5 June 1997.

Address reprint requests to Dr. Stephen G. Sligar, Director, School of Chemical Science, University of Illinois, 600 S. Mathews, Urbana, IL 61801. Tel.: 217-244-7395; Fax: 217-244-7100; E-mail: s-sligar@uiuc.edu.

0006-3495/97/09/1184/06 $2.00

MATERIALS AND METHODS

The rHDL were prepared using the sodium cholate dialysis method in molar ratios of 150:1, 175:1, and 200:1 (L-α-dipalmitoyl phosphatidylcholine: apoA-I), as described previously (Wald et al., 1990). Cholate was removed through exhaustive dialysis against 0.1 M Tris-HCl pH 8.0, 0.005% EDTA, 0.15 M NaCl, and 1 mM NaN_3. Diameters of rHDL were determined by nondenaturing 8–25% polyacrylamide gel electrophoresis. The dialysates were separated into individual rHDL classes by gel filtration on a Superdex 200 HR 10/30 column on an FPLC system (Pharmacia, Uppsala, Sweden). Three different samples were prepared, one with 2, one with 3, and one with 4 ApoA-I per rHDL, which are referred to as Lp2, Lp3, and Lp4, respectively. The variation in stoichiometry leads to a variation in the size distribution of the discoidal particles, as characterized previously by gradient gel electrophoresis, with average hydrodynamic diameters of 9.9 nm for Lp2, 14.3 nm for Lp3, and 19.2 nm for Lp4 (Wald et al., 1990). Protein concentration was determined using the method of Lowry (Lowry et al., 1951).

Purified rHDL were diluted to the desired concentration using a standard imaging buffer consisting of 10 mM $MgCl_2$, 10 mM Tris-HCl, and 0.1 M NaCl, adjusted to pH 8.0. This standard buffer was used for all AFM imaging. Muscovite mica (S and J Trading Inc., Glen Oaks, NY), previously glued to a 10-mm stainless steel disk, was freshly cleaved and 20 μl rHDL solution applied. Deposition was carried out in a clean Pyrex chamber containing additionally a pool of nanopure water (Millipore Corp., Bedford, MA) to provide humidity and seal the chamber. Samples were never allowed to dry before imaging. Some samples were rinsed with the standard imaging buffer, with no apparent change in the resultant images.

The rHDL mica was kept under buffer during transfer to the liquid cell of a Nanoscope IIIa (Digital Instruments, Santa Barbara, CA). Images were taken using either an E scanner or an A scanner, with oxide-sharpened silicon nitride tips (Digital Instruments, Santa Barbara, CA) on the thin 200-μm cantilever reported by the manufacturer to have a typical spring constant of 0.06 N/m. All images presented here were taken in the contact mode.

Deposition solutions of Lp3 rHDL were prepared with apoA-I concentrations ranging from 0.5 μg/ml to 702 μg/ml, in order to study the adsorption of rHDL to the mica surface. Height measurements of low coverage samples were taken from the center of the rHDL, while the depth of higher coverage samples was obtained using the bearing analysis routines in the Nanoscope version 4.22 software (Digital Instruments, Santa Barbara, CA). Images were obtained at forces below 100 pN with scan speeds <2 μm/s.

In order to quantitate the area per particle, images were initially processed using the Nanoscope software version 4.22 (Digital Instruments, Santa Barbara, CA), then exported to a Macintosh, running National Institutes of Health Image Version 1.60 (U.S. National Institutes of Health, Washington, DC). The area was quantitated by first generating a mask that defined the border between each single particle. A gap of three pixels was used to delineate each disk for analysis. This three-pixel gap was divided by two to obtain a gap per disk of 1.5 pixels. In order to incorporate this gap into the measured area, the circumference was multiplied by 1.5 and added to the initially measured area. This corrected area was then used in the histogram analysis. Where particles could not be resolved due to noise they were discarded, as well as any particles on the edge. Data from various images was compiled into sets using Kaleidagraph version 2.1.4 (Abelbeck Software) and fit to a two population Gaussian model using Igor Pro (Wavemetrics, Lake Oswego, OR).

Patterning and "digging" (see Results) were typically accomplished at forces of ~1 nN with scan rates of 20 to 30 Hz. Whether higher force and scan speed resulted in digging or patterning depended on the sample. The patterned image presented in Fig. 1 *F* was obtained with Lp2 rHDL present in the fluid cell in solution at an apoA-I concentration of 1.25 mg/ml.

RESULTS

Structure

While negative-stain TEM of rHDL shows many stacked, rouleaux features, it is known from a variety of other methods that this does not represent the native solution structure. We have used atomic force microscopy to address this issue by examining the structure of rHDL under physiological buffer conditions. Images also reveal a greater heterogeneity than expected from characterization of the starting preparation, and so disk size was examined in order to understand the nature of the rHDL transformations.

Measurement of particle height for each of the rHDL samples prepared (Fig. 2) resulted in a mean of 5.5 $\pm$ 0.4 nm (n = 127), which matches well with the expected value for the van der Waals layer of a DPPC bilayer, 5.6 nm (Marra and Israelachvili, 1985). While the AFM has high vertical resolution, horizontal size information is convoluted with the size of the tip. This is especially evident for small, isolated particles (Fig. 1, *A* and *B*). One method for overcoming this limitation is to calibrate the size of the tip using appropriately sized colloidal gold spheres (Xu and Arnsdorf, 1994). Effective tip calibration using this method, however, requires that the tip undergo no changes during subsequent imaging. Changes in image quality occur with a frequency that makes tip calibration very difficult, complicating the ability to quantitate the size of the individual rHDL particles.

While the AFM will distort the horizontal distances associated with single objects, the AFM is quite capable of accurately measuring the "periodicity" of a sample, since, while the tip cannot reproduce the shape of a small object correctly, it can reproduce the position of peaks and troughs. In the high coverage sample shown in Fig. 1 *D*, while the tip may distort the shape of the objects, if the border, or trough, between two rHDL can be discerned, then the area occupied by those objects can be calculated with minimal convolution of tip size. The area per particle measured in this manner will include both the particle's true area and any gaps between particles. The ratio of the area occupied by particles to the total area is the packing density.

High coverage samples were imaged at forces below 100 pN and analyzed to define an area per particle. Images were reproducible, indicating that all rearrangement processes occurred spontaneously and do not appear to be a function of low force imaging. Histograms of area per particle for all three rHDL preparations examined show a characteristic shape, resembling two distributed populations; one population which is narrow, centered at a smaller area per particle, and one population which is broad, centered at a larger area per particle (Fig. 3, *A–C*). Goodness of fit was determined by calculating the sum of the residuals squared, and for a fit to one Gaussian versus two Gaussians these values were 656 versus 371 for Lp2, 2301 versus 1004 for Lp3, and 1115 versus 684 for Lp4. Fitting the observed distributions

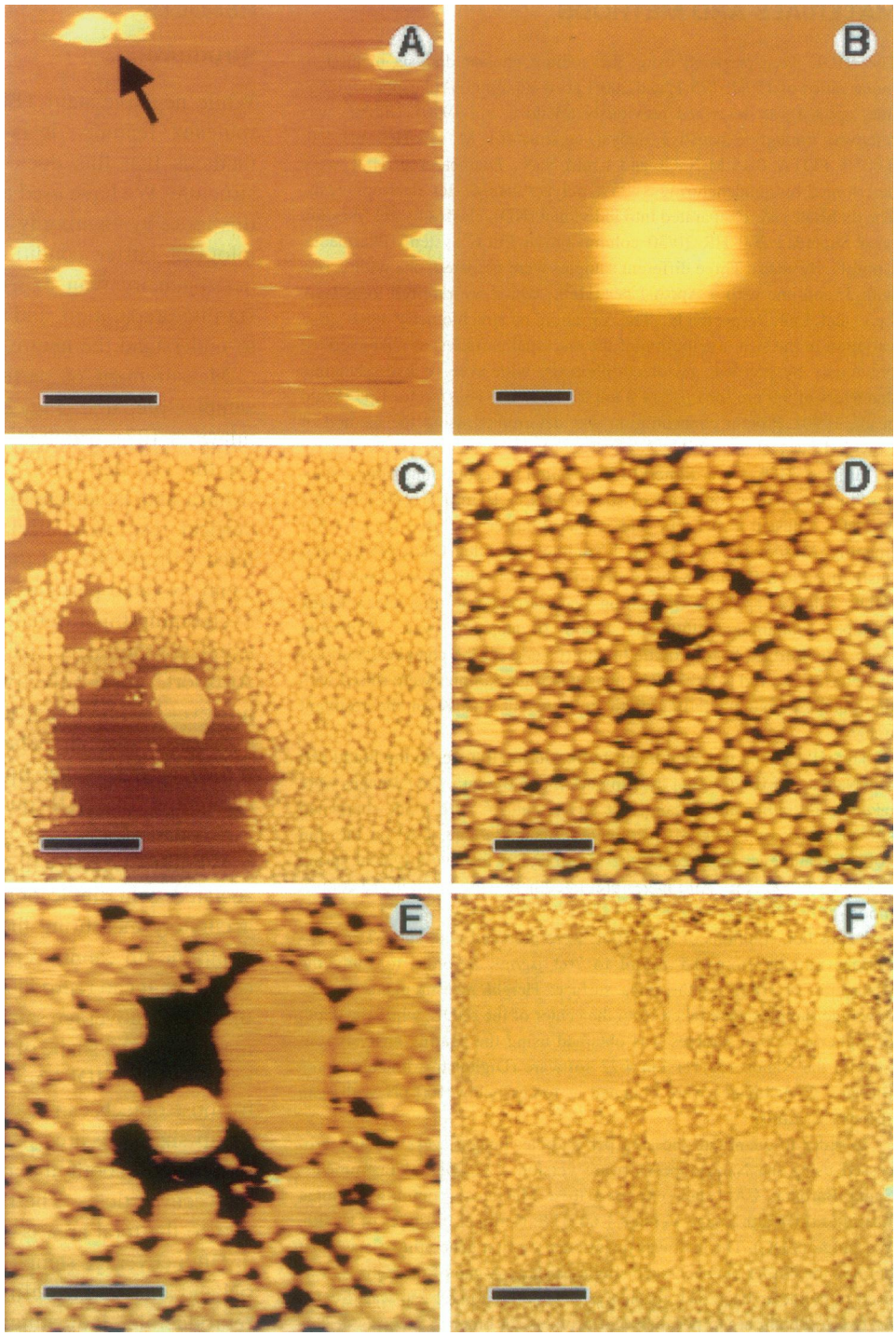

FIGURE 1 AFM images of rHDL disks. Lower coverage images are distorted by the tip. (*A*) Height mode image of low coverage rHDL disks (Lp2 rHDL). The arrow indicates grouped rHDL, as discussed in the text. (*B*) Larger image of a single rHDL disk (Lp2 rHDL). (*C*) Intermediate coverage sample, showing a large area of bare mica (Lp3 rHDL). (*D*) High coverage sample (Lp3 rHDL). (*E*) Example of digging into a high coverage sample (Lp3 rHDL). (*F*) Example of patterning a high coverage sample (Lp3 rHDL). The predefined shapes were made by controlled tip motion. Scale bars (*A*) 150 nm, (*B*) 20 nm, (*C*) 400 nm, (*D, E*) 100 nm, (*F*) 250 nm

with two Gaussians yielded the size parameters reported in Table 1.

Lipoprotein Coverage

Surfaces for imaging rHDL could be prepared with a variety of coverage levels, providing further information about the structure of the surface and the adsorption of rHDL. The coverage of the mica surface depended on the concentration of rHDL in the deposition solution. Samples prepared with 0.5 μg/ml and 8.6 μg/ml were found to have low coverage, where single Lp3 rHDL complexes could be imaged, surrounded only by bare mica (Fig. 1 *A*). Some rHDL appeared in groups, adsorbed next to each other on the mica (Fig. 1 *A*, *arrow*). Lateral force images showed trails that are due to the tip pushing the rHDL off the surface. Occasionally an

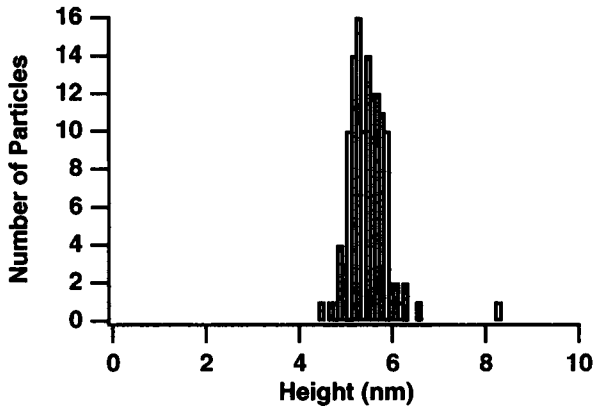

FIGURE 2 Histogram of height measurements on individual rHDL. The mean value of 5.5 ± 0.4 nm is consistent with a phospholipid bilayer structure.

rHDL could be imaged well before and after being pushed to a new location (image not shown). Many rHDL appeared incomplete, apparently because they were knocked loose from the surface during scanning.

A sample prepared at 8.6 μg/ml showed much higher coverage, with several large areas of clean mica observed in the image as well (Fig. 1 *C*). The rHDL adsorb to the mica and have similar height, indicating that they were not stacking in multilayered structures. The large rHDL present in the image serve to demonstrate the degree of heterogeneity observed. The step from the mica surface to the top of the rHDL was found to be 5.3 nm by bearing analysis.

Samples prepared at 43.0, 140, 273, and 702 μg/ml all showed high coverage, with no bare mica present (Fig. 1 *D*). The surface was quite flat, broken only by the gap between each rHDL disk. No higher features were found, which is further indication of a lack of multilayer formation. Application of a higher force allowed the tip to dig through a high coverage sample to the mica, providing a thickness measurement of 5.5 nm by bearing analysis.

The Lp2 and Lp4 rHDL could also be prepared to have either low or high coverage, with features similar to the Lp3 rHDL. High coverage samples of Lp2 rHDL were often

TABLE 1 Analysis of area per particle measurements

		Population 1		Population 2	
Sample	Expected Area (nm^2)	Area (nm^2)	FWHM (nm^2)	Area (nm^2)	FWHM (nm^2)
Lp2	79	103	47	208	352
Lp3	163	200	76	355	472
Lp4	290	343	33	789	1268

Results of the analysis of the area per particle histograms in Fig. 3, fit to a two-population model, showing peak center (Area) and full width at half-maximum (FWHM). The expected area is based on a calculation of the area of a circle using the measured Stoke's radius. Population 1 and population 2 refer to the two populations of particles discussed in the text. Note that the width of the Gaussians is not equivalent to the error of the measurements.

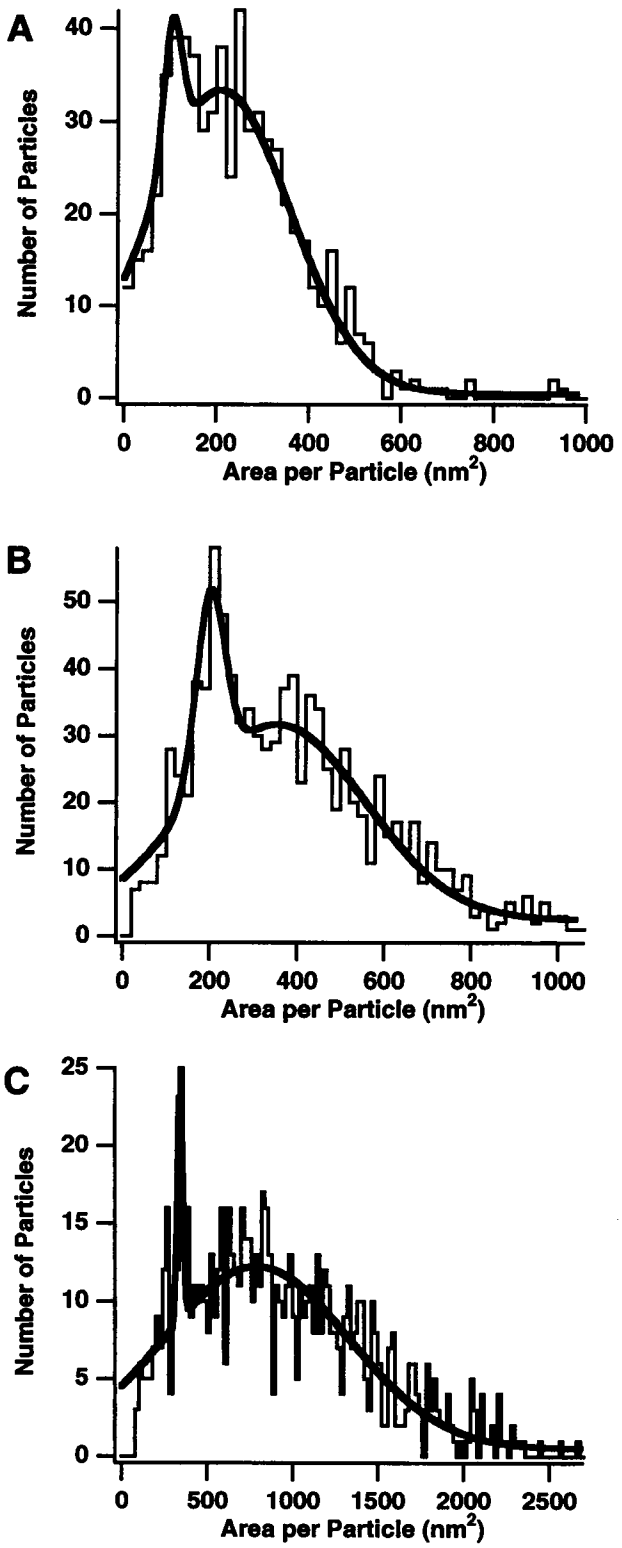

FIGURE 3 Histograms of area per particle for each sample. The solid line corresponds to a fit to two distributed populations. (*A*) Lp2 rHDL (n = 635), (*B*) Lp3 rHDL (n = 953), (*C*) Lp4 rHDL (n = 835).

very noisy and difficult to stably image, compared to Lp3 and Lp4. This may be because their smaller size results in a smaller surface with which to adsorb to the mica.

Manipulation

The imaging tip could be used to induce interparticle fusion under the right conditions. This manipulation of high coverage Lp3 rHDL allowed the various shapes in Fig. 1 *F* to be generated. Attempts to manipulate most samples resulted in a mix of patterning and digging, where the digging did not extend completely to the mica surface (based on concurrently obtained deflection data, which show more features than are found on bare mica). The "hole" in Fig. 1 *E* is 2.8 nm deep by bearing analysis, which matches the expected depth for one leaflet of a bilayer. It is not clear what the requirements for patterning are, but they probably depend on the nature of the tip and the packing of the rHDL on the surface. Recent research (Groves et al., 1996, 1997; Salafsky et al., 1996) has indicated the ability to fabricate macroscopic bilayer "corrals." Our results represent the first use of the AFM to generate this type of controlled bilayer structure, and opens up the possibility of manipulating and patterning phospholipid bilayers at the nanometer scale.

DISCUSSION

Imaging rHDL under native conditions has provided important information about the structure and interactions of these protein-lipid complexes. The concentration studies indicate that while rHDL will adsorb readily onto mica, they will not adsorb on top of each other. Given that the height of the rHDL disks is consistent with the thickness of a phospholipid bilayer, this suggests that the disks rest with the acyl chains of the phospholipid perpendicular to the mica surface. This planar ordering can be contrasted with negative-stain TEM, in which disks can be identified by their preference for stacking into rouleaux strands.

Images obtained at higher concentrations reveal a much greater heterogeneity than expected from solution studies (Fig. 1 *C*). The area per particle was examined to try to assess whether these were solution species present in low concentrations, which stand out visibly in the images only because of their size, or were the results of disk fusion and division events on the mica surface. The histograms of area per particle in Fig. 3 show two peaks, one narrow and one broad. We believe these peaks correspond to an initial, narrow population distribution, as observed in solution, and a second broad population, which is due to interdisk rearrangement events. Note that these rearrangement events are not just fusion or division, but a mix of both, resulting in the broad population that spans areas above and below the size of the initial population.

It should be noted that the width of the distributions reported in Table 1 is not equivalent to the error of the measurements. These widths correspond to a genuinely distributed population, convoluted with measurement error. This error can be estimated by considering that the piezoelectric crystals used in AFM imaging have sub-angstrom resolution, tip effects have been avoided by using high coverage samples, and the counting error associated with analysis of the images has been estimated to be <10 nm^2. Given this accuracy, it is then interesting to note that the area of the second population for Lp2 is centered at the same area as the first population for Lp3. Similarly, the second population peak for Lp3 is centered at the same area as the first population peak for Lp4. In solution, these size distributions have been found to relate directly to the number of apoA-I molecules on the edges of the disk; these results indicate that apoA-I is continuing to stabilize certain sizes of rHDL over others, even on the surface. It appears that Lp2 is converting to Lp3, and Lp3 is converting to Lp4.

By using appropriate imaging parameters, rHDL surfaces could be manipulated by the microscope tip. Manipulation of most surfaces in this fashion resulted in digging, as shown in Fig. 1 *E*, which resulted from scanning a 250-nm square area at higher force, faster scan speed, and reduced gain. The imaging parameters were reset to their typical values, and the image in Fig. 1 *E* was obtained. Digging is characterized by a fusion of some of the rHDL and removal of one sheet of the phospholipid bilayer, as determined by the observed step of 2.8 nm. Some surfaces responded, as shown in Fig. 1 *F*, with large-scale flat regions, whose shape was controlled by the tip. The difference between patterning and digging does not appear to depend on force, scan speed, or instrument gains. Typically, imaging for a few hours seemed to aid in patterning, which may indicate that adsorption of phospholipids to the tip from solution, or desorption of phospholipids from the surface, are the required step. Attempts to manipulate samples with double tips or other misshapen tips also resulted in failure. One sample resulted in total removal of the rHDL from the manipulated area, allowing visualization of the mica surface below. The parameters governing this effect are likely to be complex and will require further study to understand. Nevertheless, the ability to pattern phospholipid bilayers into controlled nanoscale domains has implications for biological sensor technology and the study of phospholipid bilayer interactions, as well as the potential to study single membrane proteins in a controlled phospholipid domain.

In summary, the work presented here represents the first images of discoidal rHDL in native conditions. These images indicate that AFM is a powerful technique for structural-functional imaging of these important biological samples. Images indicate that rHDL have a phospholipid bilayer structure. High coverage samples show that rHDL disks can undergo fusion and division events when oriented by the mica surface. Because the important reactions of lipoproteins occur on surfaces, this newly observed "fusion" process may have physiological relevance. The ability of AFM, under correct conditions, to induce this fusion to produce nanometer scale phospholipid bilayer domains has been demonstrated.

The authors thank Dr. B. Carragher for helpful discussions, and A. Weber for editorial assistance. J. Carlson is supported by a Molecular Biophysics Training grant from the National Institutes of Health.

This work was supported by National Institutes of Health Grants GM31756 (to S.G.S.) and HL16059 (to A.J.).

REFERENCES

Assman, G., A. von Eckardstein, and H. Funke. 1992. Mutations in apolipoprotein genes and HDL metabolism. *In* Structure and Function of Apolipoproteins. M. Rosseneu, editor. CRC Press, Inc., London. 87–88.

Atkinson, D., D. M. Small, and G. G. Shipley. 1980. X-ray and neutron scattering studies of plasma lipoproteins. *Ann. N. Y. Acad. Sci.* 348:284.

Atkinson, D., H. M. Smith, J. Dickson, and J. P. Austin. 1976. Interaction of apoprotein from porcine high-density lipoprotein with dimyristoyl lecithin. *Eur. J. Biochem.* 64:541–547.

Boguski, M. S., M. Freeman, N. Elshourbagy, J. M. Taylor, and J. I. Gordon. 1986. On computer-assisted analysis of biological sequences: proline punctuation, consensus sequences, and apolipoprotein repeats. *J. Lipid Res.* 33:141–166.

Brouillette, C. G., J. L. Jones, T. C. Ng, H. Kercret, B. H. Chung, and J. P. Segrest. 1984. Structural studies of apolipoprotein A-I/phosphatidylcholine recombinants by high-field proton NMR, nondenaturing gradient gel electrophoresis, and electron microscopy. *Biochemistry.* 23:359–367.

Fielding, C. J., V. G. Shore, and P. E. Fielding. 1972. Protein cofactors of lecithin: cholesterol acyltransferase. *Biochem. Biophys. Res. Commun.* 46:1493–1498.

Forte, T. M., A. V. Nichols, E. L. Gong, S. Lux, and R. I. Levy. 1971a. Electron microscopic study on reassembly of plasma high density apoprotein with various lipids. *Biochim. Biophys. Acta.* 248:381–386.

Forte, T. M., K. R. Norum, J. A. Glomset, and A. V. Nichols. 1971b. Plasma lipoproteins in familial lecithin: cholesterol acyltransferase deficiency: structure of low and high density lipoproteins as revealed by electron microscopy. *J. Clin. Invest.* 50:1141–1148.

Groves, J. T., N. Ulman, and S. G. Boxer. 1997. Micropatterning fluid lipid bilayers on solid supports. *Science.* 275:651–653.

Groves, J. T., C. Wülfing, and S. G. Boxer. 1996. Electrical manipulation of glycan-phosphatidyl inositol-tethered proteins in planar supported bilayers. *Biophys. J.* 71:2716–2723.

Hamilton, R. L., M. C. Williams, C. J. Fielding, and R. J. Havel. 1976. Discoidal bilayer structure of nascent high density lipoproteins from perfused rat liver. *J. Clin. Invest.* 58:667–680.

Jonas, A. 1986. Reconstitution of high density lipoproteins. *Methods Enzymol.* 128:553–582.

Jonas, A. 1991. Lecithin cholesterol acyltransferase in the metabolism of high density lipoproteins. *Biochim. Biophys. Acta.* 1084:205–220.

Jonas, A. 1992. Lipid-binding properties of apolipoproteins. *In* Structure and Function of Apolipoproteins. M. Rosseneu, editor. CRC Press, Inc., London. 217–250.

Jonas, A., K. Kezdy, and J. H. Wald. 1989. Defined apolipoprotein A-I conformations in reconstituted high density lipoprotein discs. *J. Biol. Chem.* 264:4818–4824.

Jonas, A., J. H. Wald, K. L. H. Toohill, E. S. Krul, and K. Kezdy. 1990. Apolipoprotein A-1 structure and lipid properties in homogeneous, recombinant spherical and discoidal high-density lipoproteins. *J. Biol. Chem.* 265:22123–22129.

Lowry, O. H., N. J. Rosebrough, A. L. Farr, and R. J. Randall. 1951. *J. Biol. Chem.* 193:265–275.

Marra, J., and J. Israelachvili. 1985. Direct measurement of forces between phosphatidylcholine and phosphatidylethanolamine bilayers in aqueous electrolyte solutions. *Biochemistry.* 24:4608–4618.

Matz, C., and A. Jonas. 1982. Micellar complexes of human apolipoprotein A-I with phosphatidyl cholines and cholesterol prepared from cholate lipid dispersions. *J. Biol. Chem.* 257:4535–4540.

Morrissett, J. D., J. G. Gallagher, K. C. Aune, and A. M. Gotto. 1974. Structure of the major complex formed by interaction of phosphatidylcholine bilamellar vesicles and apolipoprotein-alanin (Apo-C-III). *Biochemistry.* 13:4765–4771.

Salafsky, J., J. T. Groves, and S. G. Boxer. 1996. Architecture and function of membrane proteins in planar supported bilayers: a study with photosynthetic reaction centers. *Biochemistry.* 35:14773–14781.

Segrest, J. P. 1977. Amphipathic helixes and plasma lipoproteins: thermodynamic and geometric considerations. *Chem. Phys. Lipids.* 18:7–22.

Segrest, J. P., M. K. Jones, H. De Loof, C. G. Brouillette, Y. V. Venkatachalapathi, and G. M. Anantharamaiah. 1992. The amphipathic helix in the exchangeable apolipoproteins: a review of secondary structure and function. *J. Lipid Res.* 33:141–165.

Tall, A. R., D. M. Small, R. J. Deckelbaum, and G. G. Shipley. 1977. Structure and thermodynamic properties of high density lipoprotein recombinants. *J. Biol. Chem.* 252:4701–4711.

Wald, J. H., E. S. Krul, and A. Jonas. 1990. Structure of apolipoprotein A-I in three homogeneous, reconstituted high density lipoprotein particles. *J. Biol. Chem.* 265:20037–20043.

Wlodawer, A., J. P. Segrest, B. H. Chung, R. Chiovetti, and J. N. Weinstein. 1979. High-density lipoprotein recombinants: evidence for a bicycle tire micelle structure obtained by neutron scattering and electron microscopy. *FEBS Lett.* 104:231–235.

Xu, S., and M. F. Arnsdorf. 1994. Calibration of scanning (atomic) force microscope with gold particles. *J. Microscopy.* 173, Pt. 3:199–210.